Reconstruction-Based Estimation of the Scatter Component in Positron Emission Tomography

Habib Zaidi

Division of Nuclear Medicine, Geneva University Hospital, Switzerland

A new method to assess the scatter component in positron emission tomography (PET) based on estimating the low-frequency component corresponding to scattered events using ordered subsets - expectation maximization (OSEM) reconstructions is proposed in this paper and evaluated using Monte Carlo simulation studies, experimental phantom measurements and clinical studies. The rationale of this method called Statistical Reconstruction-Based Scatter Correction (SRBSC) is that the image corresponding to scattered events in the projection data consists of almost low-frequency components of activity distribution and that the low-frequency components will converge faster than the high-frequency ones in successive iterations of statistical reconstruction methods such as OSEM. The second assumption is that the high-frequency components will be smeared, i.e. filtered by the scatter response kernels. A simple model has been devised to parameterize the scatter component using Monte Carlo simulations. The unscattered component estimated using SRBSC was compared to the true unscattered component as estimated by Monte Carlo simulations for simple phantom geometries and clinically realistic source distributions. Quantitative analysis was also performed on reconstructed images using simple metrics like the contrast, absolute concentration, recovery coefficient and signal-to-noise ratio. The SRBSC method tends to undercorrect for scatter in most regions of the 3D Hoffman brain phantom, but gives good activity recovery values which average within 1%. It was concluded that the proposed method improves image quality and the contrast compared to the case where no correction is applied and that an accurate modeling of the scatter component is essential for a proper scatter correction.

Key words: PET, scatter correction, OSEM, Monte Carlo

Ann Nucl Med Sci 2001;14:161-172

Introduction

One of the obstacles to the use of volume imaging positron emission tomography (PET) scanners is the increase in the scatter fraction which influences the quantitative accuracy and represents from 30% to 50% of the data acquired in 3D mode. The inclusion of Compton-scattered events degrades image quality and might in some cases reduce diagnostic accuracy. In addition to a decrease in the image contrast, events may also appear in regions of the image where there is no activity (e.g. outside the patient). Scattered photons arise from the whole attenuating medium, including the imaging table and the PET tomograph itself.

Accurate 3D reconstruction in PET requires compensation for the effects of attenuation and scatter. The problem of Compton scatter in 3D PET is far more complicated to solve than attenuation [1]. The issue of scatter detection, modeling and correction are addressed in many publications [2-8]. Implicit in all scatter correction methods in nuclear imaging is the existence of some complementary degradation model

Received 12/27/2000; revised 2/26/2001; accepted 3/14/2001.
For correspondence or reprints contact: Habib Zaidi, Ph.D., Division of Nuclear Medicine, Geneva University Hospital, CH-1211 Geneva, Switzerland. Tel: 41 22 372 72 58, Fax: 41 22 372 71 69, E-mail: habib.zaidi@hcuge.ch

describing the nature and processes giving rise to detected scattered events. The general lack of theoretical connection between the degradation and correction models raises several important questions about the status of the outcome of scattered events and the formulation of the required scatter correction models. The problem of scatter correction is of paramount importance in high-resolution PET imaging in which the scatter degradation features become more complex.

Over the last two decades, many scatter correction methods in PET and single-photon emission tomography (SPECT) have been developed for the purpose of reducing the resultant degradation of image contrast and loss of quantitative accuracy. Simple and more sophisticated scatter correction techniques have their own advantages and drawbacks. Most of these methods attempt to estimate the scatter contamination and then remove it using either subtraction or deconvolution techniques. There have been a number of studies comparing these methods in SPECT [9,10] and PET [11,12] imaging. The primary concerns affecting these methods are: (i) the scatter estimates may be inaccurate, leading to bias in the reconstructed image; and (ii) the scatter compensation is often accompanied by a substantial increase in statistical noise. In addition, many of the methods require estimating parameters that may change for each patient and imaging protocol. Some scatter compensation methods incorporate scatter in the transition matrix or point-spread function during iterative reconstruction. It has been shown that this can lead to highly quantitative accuracy [4,13] and improved signal-to-noise ratio in the reconstructed images [5]. With the advent of faster computers and accelerated iterative reconstruction algorithms, different approaches to scatter compensation are receiving much attention.

A new scatter correction method called Statistical Reconstruction-Based Scatter Correction (SRBSC) in which the low-frequency component corresponding to scatter events is estimated using OSEM reconstructions is proposed in this paper and evaluated using Monte Carlo simulation studies, experimental phantoms and clinical data. A comparative assessment of the relative performance of this method against more common correction methods was also conducted and summarized in another publication [14].

Theory

Reconstruction-based scatter compensation is a technique in which the scatter response function is modeled during the reconstruction process. Several research groups devised different algorithms belonging to this class of methods for SPECT [4,5,13,15,16]. The proposal to include scatter estimation in iterative reconstruction is original in PET. Up to now, its feasibility in 3D PET was hampered by the heavy computational load of scatter estimation models. In this section, a new technique for scatter correction in 3D PET is proposed. Other investigators independently reported a related method for scatter correction in SPECT imaging [17]. The principle of the method is based on the hypothesis that the image corresponding to scattered events in the projection data consist of almost low-frequency components of activity distribution and that the low-frequency components will converge faster than the high-frequency ones in successive iterations of statistical reconstruction methods such as the maximum likelihood - expectation maximization (MLEM) or its accelerated version, the ordered subsets - expectation maximization (OSEM), which is given by the following equation:

$$f^{n+1} = \frac{f^{n}}{sensitivity} \times backproj\left[\frac{p}{fwdproj(f^{n})}\right] \quad (1)$$

where f denotes the source distribution, p the measured projection data, n the iteration number, and *fwdproj* and *backproj* are the forward and back projection operators which are carried out throughout iterative algorithms implementation. Their accurate and efficient computation is crucial to the accuracy, effectiveness and speed of the algorithms. The *sensitivity* image computes the probability that an event emitted in a given voxel is detected or not. For current generation PET scanners, the number of elements can be prohibitively large even after symmetry reduction.

A well-known fact is that iterative reconstruction algorithms possess a non-uniform convergence property [18]. That is, low-frequency components of the image tend to be recovered earlier in iterative reconstruction than high-frequency components which contain a large amount of noise. There has been some evidence presented by other researchers

supporting this hypothesis [19]. The study of convergence properties of the MLEM algorithm by Fourier analysis revealed clearly the non-uniform frequency response of the EM algorithm [18]. Moreover, preliminary investigations of inverse Monte Carlo-based reconstruction indicate that the recovery of spatial frequency information is achieved at different numbers of iterations for different spatial frequencies: higher spatial frequencies appear at higher iterations while the lower frequencies (smooth structures) are well defined at early iterations [13].

The distribution of scattered photons in nuclear imaging (SPECT and PET) has been studied extensively [20-22]. In terms of the frequency response, the scatter components of PET projection data tend to be dominated by low-frequency information, though there is some middle- and high-frequency information present. The SRBSC approach takes advantage of this by estimating the scatter component from forward projection of images reconstructed in early iterations of OSEM.

The method we propose estimates the scatter distribution from these forward projected data. A pure additive model of the imaging system is assumed here where the recorded data are composed of an unscattered and a scattered component plus a noise term due to statistical fluctuations, and can be written in the following form [21]:

$$P_0 = P_u + P_s + \eta \qquad (2)$$

where p_o are the observed data, p_u and p_s are the unscattered and scattered components respectively, and η is the noise term. The problem to be addressed consists in estimating the unscattered distribution (p_u) from the measured data (p_o) contaminated by scatter, or alternatively estimate the scattered component (p_s) and then derive p_u. The observed data can be modeled as a convolution of the source distribution with the system response function. The total response function of the scanner can be divided in two response kernels corresponding to the scattered and unscattered components, *srf* and *urf*, respectively. For modeling purposes, two assumptions can be made: the stationary and nonstationary assumptions. In the stationary assumption, the scatter is assumed to be analytically defined and not dependent on the object, activity distribution, etc. The nonstationary assumption overcomes this problem by taking into consideration the dependence of scatter upon source locations, object size, detector angle, etc. Using the additive imaging model combined with the stationary assumption and neglecting statistical noise, the measured data can be related to the true activity distribution (f) by the convolution relation:

$$P_0 = fwdproject(f) \otimes (urf + suf) = p_u + p_s \qquad (3)$$

where $\otimes$ denotes the convolution operator. Within the limits of our assumptions, the activity distribution, f, can be roughly divided in two parts:

$$f = f_L + f_H \qquad (4)$$

where f_L denotes the low-frequency image and f_H the high-frequency one. The range of low-frequency components is assumed to be equivalent to the frequency range corresponding to the scatter component p_s as detailed in the following derivation of the method. In PET, the scatter response kernels extend far outside the source activity, i.e. contain low-frequency components while the unscatter response kernels are limited to a small region corresponding to the location of the source distribution. Thus, the scatter components correspond to the low-frequency range in the source distribution. Based on the assumption that the high-frequency components will be smeared, i.e. filtered by the scatter response kernels, the scatter components in the projection data can be approximated as follows:

$$\begin{aligned} p_s &= [fwdproject(f_L) + fwdproject(f_H)] \otimes srf \\ &\approx fwdproject(f_L) \otimes srf \end{aligned} \qquad (5)$$

The proposed SRBSC method for scatter correction exploits the properties mentioned above. Figure 1 shows a flow chart of the general principles of the method. The basic steps followed when applying the method consist of the following:

(1) estimate the low-frequency components by only one OSEM iteration;
(2) obtain the scatter components by forward projection of

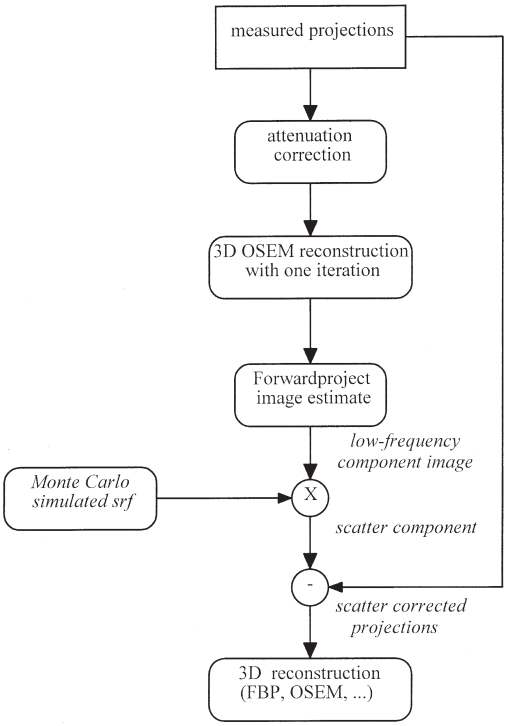

Figure 1. Flow-chart illustrating the general principles of statistical reconstruction-based scatter correction (SRBSC) technique

the estimated image convolved with appropriate measured or Monte Carlo simulated scatter response kernel *srf*;

(3) subtract the estimated scatter components scaled by the SF from measured projections;

(4) reconstruct the image using any available reconstruction algorithm (analytic, iterative) using scatter corrected projection data.

The scatter distribution is modeled as the convolution of the forward projected data with the scatter response function on the 2D projections. As opposed to the convolution-subtraction method which operates on projection data highly contaminated by scatter and requires several iterations to produce acceptable results, the present method estimates the scatter distribution in the image space in a single-pass process but requires an additional forward projection step. This allows avoiding the non-linear behaviour of iterative scatter compensation methods.

Methods

Parameterization of Scatter Component

To characterize scattered radiation in 3D PET, experimental phantom studies and Monte Carlo simulations have been extensively used in different imaging situations and scanning conditions. The Monte Carlo method has proven to be very useful for modeling the scatter response function (*srf*) [20-24]. However, on-the-fly calculations for each patient is still a dream with current desktop computers available in PET centers, which renders the clinical routine implementation of such an approach impractical. In a previous paper, we described a simple method for analytically estimating the scatter component in the projection data for a known source and uniform attenuating medium as a scatter model [22]. Three possible applications of this scatter model are forward-projection of the data for use in iterative reconstruction-based scatter compensation, the analytic generation of simulated projection data for applications requiring large numbers of data sets of different projection data such as observer studies or training of neural networks, and position-dependent scatter kernels for non-stationary convolution subtraction-based scatter correction methods [2-3,20]. The parameterization of the scatter distribution function is performed by fitting simulated response functions to a line source with mono-exponential kernels. The scatter fractions were also parameterized by a simple fitting function.

The 3D OSEM Reconstruction Software

The EM algorithm is applied in emission tomography as an iterative technique for computing maximum likelihood estimates of the activity density parameters. Hudson and Larkin [25] presented an accelerated version of the EM algorithm based on an ordered sets approach. The OSEM algorithm processes the data in subsets (blocks) within each iteration; this procedure accelerates convergence by a factor proportional to the number of subsets. Many independent tests proved that OSEM produces images which are similar in quality to those produced by the EM algorithm in a fraction of the time.

A software implementation of OSEM [26] using a flexible and modular object-oriented library for 3D PET reconstruction [27] was used. The algorithm combines the forward

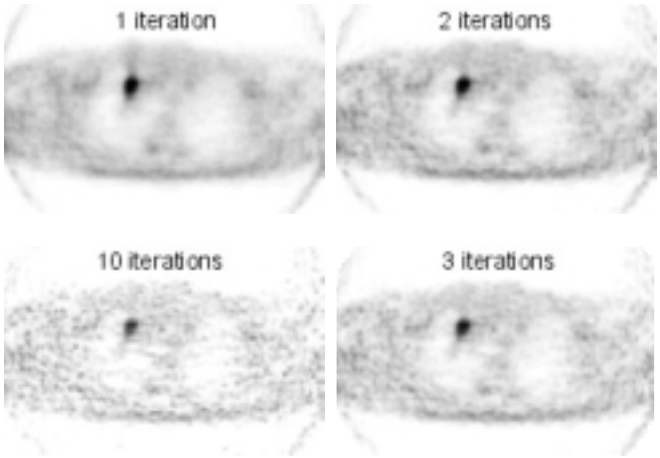

Figure 2. OSEM reconstructions of a PRT-1 oncology study at the level of the thorax using 24 subsets and different numbers of iterations: they are from top left, clockwise: one full iteration, 2 iterations, 3 iterations, and 10 iterations, respectively

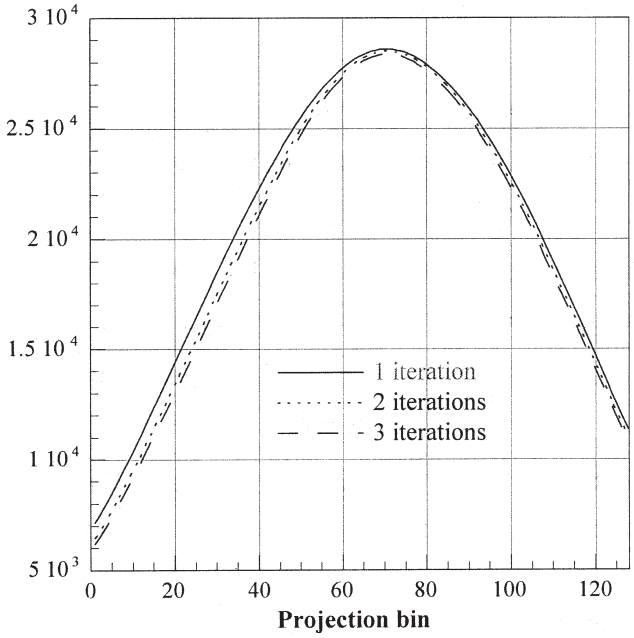

Figure 3. Profile of the scatter component in a projection plane of the clinical oncology study estimated by SRBSC using 2 subsets with one (solid line), two (dotted line) and three full iterations (dashed line) of OSEM

and backprojection operators with an appropriate choice of ordered sets to fully use all symmetry properties for fast computation. There are various choices for the first estimate of the source distribution such as a uniform field, or an image obtained from earlier iterations or another reconstruction algorithm such as filtered backprojection. Some groups reported that the use of the backprojection of the measured data as the first estimate is a good starting point. Our investigations did not confirm these observations, thus we used a uniform image as a first estimate.

To confirm the fast convergence properties of the low-frequency components in statistical reconstructions, a clinical oncology study was reconstructed using 24 subsets with 1, 2, 3 and 10 full iterations of OSEM. This study was reconstructed by pure OSEM without iterative or post-filtering. Figure 2 illustrates a slice reconstructed with different numbers of iterations. It can be noticed that the quality of the images is degraded when the number of iterations is increased up to 10 where the MLEM solution starts to diverge. This is a well-known phenomenon in iterative reconstruction and may be explained by the fact that OSEM is based on convergence of the reprojected data of estimated images to the measured noisy projections. Therefore, the reconstructions will converge to noisy images and may diverge from the solution image when we increase the number of iterations.

The scatter components converge very rapidly in the first iterations of OSEM. Figure 3 shows the profiles of scatter distribution in one sinogram plane as estimated by the SRBSC method after 1, 2 and 3 iterations of OSEM using 2 subsets. No appreciable differences are visible on the plot. Similar results have been obtained on other projection planes. This indicates that the estimated scatter components converge in the first iterations of OSEM and has some interesting practical consequences, the most important being that one iteration of OSEM is sufficient to assess the distribution of low-frequency scatter. This property makes the method very fast, which renders its implementation in clinical routine viable.

Phantom Simulations, Experimental and Clinical Studies

Scatter correction techniques can be evaluated using Monte Carlo simulation studies, experimental phantom measurements, or clinical studies. Monte Carlo simulation is extremely useful as it allows separating scattered and unscattered events and comparing the estimated and true scatter components. Previously reported Monte Carlo validations of

scatter correction techniques and related parameters have often been made by using simple source, attenuating medium geometries and compositions. In addition to these evaluations, there is also need to investigate more clinically realistic source distributions to validate and compare scatter correction techniques. An evaluation of the relative performance of this method was performed using measurements of a physical Hoffman 3D brain phantom (Data Spectrum Corp., Hillsborough, NC, USA) with a grey-to-white matter ratio of 5:1 and Monte Carlo simulated data of a 3D digital brain phantom [28]. Evaluations have also been performed for the Utah phantom [29] to characterize the method for more standard geometries and allow determination of whether performance in the standard geometry predicts performance in the clinically realistic source distribution. The unscattered component in the simulated projection data was recorded and used as a reference to which the corrected projections using SRBSC were compared.

A calculated attenuation correction using a constant linear attenuation factor ($\mu = 0.096$ cm^{-1}) was used for simulated phantoms. Transmission data using ^{68}Ge rotating rod sources were used instead in the experimental phantoms and clinical studies. The 3D attenuation correction files are created by forward projection through the reconstructed 2D attenuation map. The reprojection method (3DRP) [30] was used to reconstruct the data sets with and without applying the scatter correction technique. The maximum acceptance angle used for 3D reconstructions corresponds to 6.2˚.

Well-established metrics are used to assess image quality. This includes calculations of the contrast and absolute concentrations measured in the different compartments of the Utah phantom, the signal-to-noise ratio and the recovery coefficient. Different regions of interest (ROIs) were defined and the average number of events within each ROI computed for both ideal, non-corrected and scatter corrected images. The Hoffman brain simulation was evaluated by calculating the activity recovery for 13 irregular ROIs over structures that are of special importance in neuroanatomy. The image slice used for calculating the ROIs was the one including the basal ganglia [14].

The proposed scatter correction algorithm was also tested on clinical data obtained on the PRT-1 scanner from the Geneva University Hospital [31]. This is a BGO-based partial-ring rotating 3D only tomograph. Cerebral and oncology clinical studies were selected from the database and used for clinical evaluation of the scatter correction method.

Results

Figure 4 shows a comparison of a profile through a sinogram plane representing the true unscattered component as estimated by the Monte Carlo simulations and by the scatter correction procedure for both the Utah phantom and the 3D Hoffman brain phantom. The scatter correction technique gives a reasonable estimation of the unscattered component

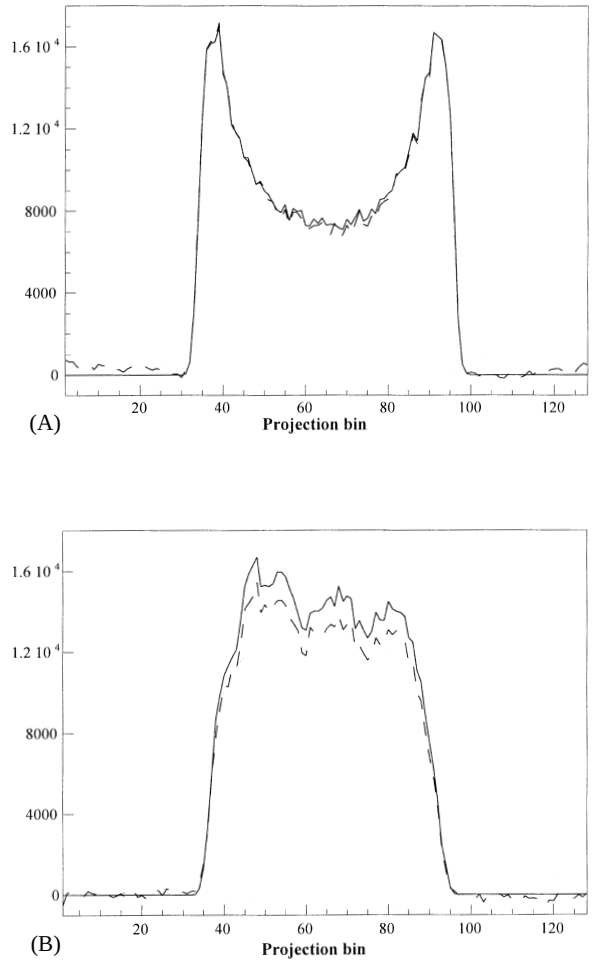

Figure 4. Integral profiles through a sinogram plane of the simulated unscattered component (solid line) and the scatter corrected sinogram using SRBSC (dashed line) for (A) the Utah phantom (B) and the 3D Hoffman brain phantom

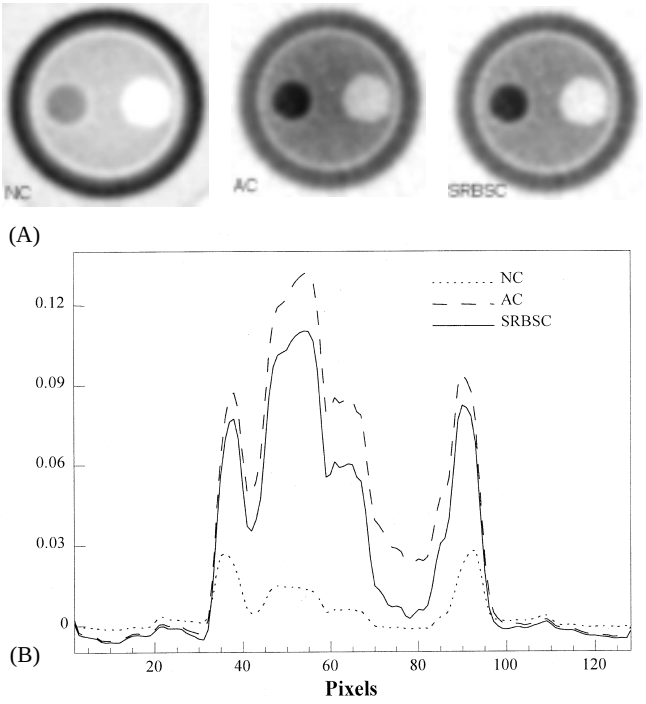

Figure 5. (A) Reconstructed images of the physical Utah phantom with activity in the outer compartment (out of field-of-view activity). The images shown are: NC (left), AC (center), and SRBSC (right). (B) Horizontal profiles through the centre of the image illustrated in (A): NC (dotted line), AC (dashed line), and SRBSC (solid line)

and successfully brings the activity to zero faster outside the object. A better estimation of the unscattered component can be seen for the simple geometrical Utah phantom with a uniform source distribution than for the Hoffman brain phantom with a complex source distribution.

The reconstructed images of the physical Utah phantom with activity in the outer compartment are shown in Figure 5. Horizontal profiles through the images are also illustrated. The scatter correction technique improves the quality of the images and allows a better definition of the cold cylinder (right small cylinder in Figure 5) compared to the case where only attenuation correction is applied, however, the images appear noisier after scatter subtraction. The results of the quantitative analysis of the data corresponding to figure 5 are summarized in Table 1. Obviously, the scatter correction method improves the contrast and absolute quantification compared to the case where no correction is applied without significantly increasing the noise. It has been shown that the SRBSC method predicts reasonably well the contrast and that statistical noise is insignificantly changed even when a significant amount of scatter is originating from outside the FOV.

Table 2 shows the results of the quantitative evaluations of the percentage activity recovery before and after applying the scatter correction technique for the 13 irregular ROIs, which cover important structures of the brain [14]. The SRBSC technique tends to undercorrect for scatter in most regions but gives very good activity recovery values, which average within 1%. The effect of scatter removal in areas where no activity is present (e.g. CSF) is clearly seen and the contrast between grey and white matter is improved and the structures are more clearly delineated (not shown). Results obtained using the SRBSC approach for scatter correction in cerebral 3D PET scans (homogeneous attenuating region) seem to be accurate and well adapted to this kind of studies [14].

Figure 6 illustrates a slice from the uncorrected and scatter corrected 3D clinical study at the level of the thorax. It should be noted that for the whole-body, it is difficult to assess the effect of the scatter correction on the images

Table 1. Absolute concentrations and contrast measured in the different compartments of the scanned Utah phantom with attenuation correction only (AC) and after applying the scatter correction technique (SRBSC). The mean and standard deviations are shown. The signal-to-noise ratio (SNR) measured in the background (A) is also shown. The outer compartment (E) was filled with activity concentration equal to that in the background region

Figure of merit	Absolute concentration (kBq/ml)		Contrast (%)	SNR
Case/Compartment	B	D	C	A
Calibration concentration	5.88	4.86	100	—
AC	7.94±0.3	5.47±0.2	64.60±1.1	19.04±4.7
SRBSC	6.76±0.3	4.90±0.2	86.78±3.3	16.81±4.6

Table 2. Percentage recovery calculated in different structures of clinical interest in the Hoffman 3D brain phantom with attenuation correction only (AC) and after applying the scatter correction technique (SRBSC). The average and standard deviation (s.d.) for all the ROIs are also shown

	Recovery (%)	
ROI	AC	SRBSC
R1	110.8±0.8	101.7±0.2
R2	113.5±1.1	101.0±0.3
R3	114.9±1.3	100.1±0.3
R4	113.9±0.2	100.4±0.1
R5	119.7±1.0	100.6±0.3
R6	122.2±1.3	100.7±0.6
R7	111.1±0.5	101.5±0.0
R8	113.8±0.5	100.9±0.1
R9	113.5±0.2	100.4±0.1
R10	112.7±0.1	100.6±0.1
R11	120.9±1.1	101.1±0.5
R12	121.8±0.8	100.5±0.1
R13	122.5±1.5	103.3±1.1
Average	116.2	101.0
s.d.	4.4	0.8

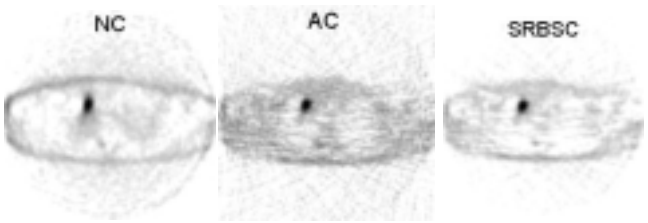

Figure 6. Reconstructed images of an oncology study at the level of the thorax. The images shown are from left to right: NC, AC, SRBSC, respectively

shown. However, the streak artefacts seen in the attenuation corrected image only have been reduced after scatter subtraction. The physics of photon interactions indicates that in a low-density region, the amount of scattering is negligible. However, many incorrectly positioned LORs will be assigned to projection data through the low-density region with similar probabilities to an adjacent, more dense region, as a result of the coincidence detection method [21]. This is a possible explanation for the fact that the presence of a small, low-density region will hardly be visible on the scatter profile in the projection data. However, for obvious reasons, the measured attenuation correction factors applied to this low-density region will be lower. The resulting effect after reconstruction is the underestimation of scatter contribution from this region. This illustrates one of the possible interactions of scatter correction with the other correction and processing techniques (e.g. attenuation).

Discussion and Conclusions

The image quality of PET reconstructions is degraded by a number of physical factors including: (1) the attenuation of the photons travelling towards the detector; (2) the detection of scattered as well as primary photons; (3) the finite spatial resolution of the imaging system; (4) the limited number of counts one is able to collect when imaging patients; and (5) physiological, as well as patient motion. While the quantitative accuracy of 3D PET is limited mainly by attenuation and scatter corrections, it may also be influenced by the choice of the reconstruction algorithm. It is important to know both systematic and statistical errors in activity quantification when using different reconstruction algorithms. Historically, once one had obtained the best projection data feasible, one typically applied compensations for these degradations either prior to or after reconstruction with filtered backprojection. Currently, the preferred compensation strategy is becoming the incorporation of modeling these degradations into an iterative reconstruction method. This trend is likely to continue into the future, and these methods become routinely employed clinically.

Much research and development has been concentrated on the scatter compensation required for quantitative 3D PET. Increasingly sophisticated scatter correction procedures are under investigation; particularly those based on accurate scatter models, and iterative reconstruction-based scatter compensation approaches. Monte Carlo methods give further insight and might in themselves offer a possible correction procedure [32]. The main difference among the correction methods is the way in which the scatter component in the selected energy window is estimated. The most reliable method to determine the actual amount of scatter in the image is physical modelling of the scatter process to resolve the observed energy spectrum into its unscattered and scattered components. By observing how accurately a scatter correction algorithm estimates the amount and distribution of

scatter under conditions where it can be accurately measured or otherwise independently determined, it is possible to optimize scatter correction techniques. A number of scatter correction techniques have been proposed and successfully implemented in 3D PET [2-4, 6-8,32]. Approximately exact modeling in iterative reconstruction may become the method of choice as computing times and algorithms continue to improve. It is worth to note that most research performed in this area is concentrated in the field of SPECT imaging [5,16,33]. Application of this class of algorithms in PET is highly desired.

Scatter corrected images have poorer signal-to-noise ratio illustrated by a decrease of the signal-to-noise ratio, which can be explained by the scatter subtraction process and the reduction of the statistics in the acquired data sets. However, the quantitative accuracy is greatly improved. A remarkable enhancement of the contrast in the different compartments of the Utah phantom (Table 1) and the recovery coefficient in the different structures of the 3D Hoffman brain phantom (Table 2) are noticed after scatter subtraction. The immunity to noise in emission data of statistical reconstruction-based scatter correction methods makes them particularly applicable to low-count emission studies.

Contribution of scatter from outside the FOV is a challenging issue that needs to be addressed with large axial FOV 3D PET scanners. The dual-energy window method [6] was reported to be more successful in correcting for scatter originating from outside the FOV [11]. The SRBSC technique estimates the scatter directly from measured data whereas the dual-energy window method is sensitive to contributions from both in- and out-of-FOV activity. Nevertheless, it is believed that this is not a major problem in cerebral studies and small axial FOV tomographs. The problem remains crucial for abdominal and thoracic studies where contribution of scatter from outside the FOV is not negligible.

For the data presented in this paper, OSEM reconstructions were performed using 2 subsets to estimate the scatter component. The method is sensitive to the number of subsets chosen to reconstruct the low-frequency image. For a large number of subsets, one iteration of OSEM do not provide a low-frequency image, in which case the forward projection will be almost identical to the measured projection data. The SRBSC approach is computationally efficient as it can be easily implemented on vector or parallel computing hardware and the software required either for forward projection or fast Fourier transform is widely available in the public domain. Moreover, the low spatial frequency nature of the scatter distribution allows reducing the data size by coarse rebinning in the radial and axial direction without sacrificing the accuracy in the scatter distribution estimation [16].

The statistical errors in the scatter corrected data have not been fully investigated. The error propagation has not been fully analysed and therefore no error limits have been given. In order to fully assess the characteristics of the SRBSC method, further evaluation of the uncertainty needs to be made. It is concluded that the present method improves the contrast compared to the case when no correction is applied and that an accurate modelling of the scatter component is essential for a proper scatter correction. Moreover, it performs slightly better than the convolution-subtraction method [3] and provides better signal-to-noise ratio [14].

The method has already been applied in SPECT imaging [17]. We believe that the basic principles of the method could also be applied to other scanner geometries including dual-head coincidence gamma cameras and the combined PET/CT system as well as to other imaging modalities such as transmission CT and combined SPECT/CT. However, the success of such applications will depend on the efficient and accurate calculation of scatter responses from objects with non-uniform density. Completion of the proposed SRBSC algorithm for scatter correction by including accurate models for detector efficiency, multiple scatters, scatter from outside the field-of-view and a number of minor improvements would enable quantitative, fully 3D PET imaging in the head and the body.

Acknowledgments

This work was supported in part by the Swiss Federal Office for Education and Science under grant 96.193 within the European Esprit LTR project PARAPET (EP23493) and the Swiss National Science Foundation under grant SNSF 3152-062008. The author gratefully thanks Dr. Dale Bailey for fruitful discussions and useful comments; partners of the PARAPET project especially MRC Cyclotron Unit, UK, for

supplying the experimental data sets, and the staff of the nuclear medicine division at Geneva University Hospital.

References

1. Thompson CJ. The problem of scatter correction in positron volume imaging. IEEE Trans Med Imag 1993;12:124-132.
2. Shao L, Karp JS. Cross-plane scattering correction - point source deconvolution in PET. IEEE Trans Med Imag 1991;10:234-239.
3. Bailey DL, Meikle SR. A convolution-subtraction scatter correction method for 3D PET Phys Med Biol 1994;39:411-424.
4. Frey EC, Tsui BMW. A fast projector-backprojector pair modeling the asymmetric, spatially varying scatter response function for scatter compensation in SPECT imaging. IEEE Trans Nucl Sci 1993;40:1192-1197.
5. Beekman FJ, Kamphuis C, Frey EC. Scatter compensation methods in 3D iterative SPECT reconstruction: a simulation study. Phys Med Biol 1997;42:1619-1632.
6. Grootoonk S, Spinks TJ, Sashin D, Spyrou NM, Jones T. Correction for scatter in 3D brain PET using a dual energy window method. Phys Med Biol 1996;41:2757-2774.
7. Ollinger JM. Model-based scatter correction for fully 3D PET. Phys Med Biol 1996;41:153-176.
8. Watson CC, Newport D, Casey ME, deKemp A, Beanlands RS, Schmand M. Evaluation of simulation-based scatter correction for 3-D PET cardiac imaging. IEEE Trans Nucl Sci 1997;44:90-97.
9. el Fakhri GN, Buvat I, Pelegrini M, et al. Respective roles of scatter, attenuation, depth-dependent collimator response and finite spatial resolution in cardiac single-photon emission tomography quantitation: a Monte Carlo study. Eur J Nucl Med 1999;26:437-446.
10. Ljungberg M, King MA, Hademenos GJ, Strand SE. Comparison of four scatter correction methods using Monte Carlo simulated source distributions. J Nucl Med 1994;35:143-151.
11. Townsend DW, Price JC, Mintun MA, et al. Scatter correction for brain receptor quantitation in 3D PET. In: Myers R, Cunningham VJ, Bailey DL, Jones T, eds. Quantification of Brain Function Using PET. San Diego: Academic Press; 1996:76-81.
12. Sossi V, Oakes TR, Ruth TJ. A phantom study evaluating the quantitative aspect of 3D PET imaging of the brain. Phys Med Biol 1998;43:2615-2630.
13. Floyd CE Jr, Jaszczak RJ, Greer KL, Coleman RE. Inverse Monte Carlo as a unified reconstruction algorithm for ECT. J Nucl Med 1986;27:1577-1585.
14. Zaidi H. Comparative evaluation of scatter correction techniques in 3D PET. Eur J Nucl Med 2000;27:1813-1826.
15. Bowsher JE, Floyd CE Jr. Treatment of Compton scattering in maximum-likelihood, expectation-maximization reconstructions of SPECT images. J Nucl Med 1991;32:1285-1291.
16. Kadrmas DJ, Frey EC, Karimi SS, Tsui BM. Fast implementations of reconstruction-based scatter compensation in fully 3D SPECT image reconstruction. Phys Med Biol 1998;43:857-873.
17. Liu Z, Obi T, Yamaguchi M, Ohyama N. Fast estimation of scatter components using the ordered subsets expectation maximization algorithm for scatter compensation. Opt Rev 1999;6:415-423.
18. Tanaka E. A fast reconstruction algorithm for stationary positron emission tomography based on a modified EM algorithm. IEEE Trans Med Imag 1987;6:98-105.
19. Pan TS, Yagle AE. Numerical study of multigrid implementations of some iterative image reconstruction algorithms. IEEE Trans Med Imag 1991;10:572-588.
20. Ljungberg M, Strand SE. Scatter and attenuation correction in SPECT using density maps and Monte Carlo simulated scatter functions. J Nucl Med 1990;31:1560-1567.
21. Bailey DL, et al. Quantitative procedures in 3D PET. In: Bendriem B, Townsend DW, eds. The Theory and Practice of 3D PET. The Netherlands: Kluwer Academic Publishers; 1998:55-109.
22. Zaidi H. Statistical reconstruction-based scatter correction: a new method for 3D PET. Conference Proceedings of the World Congress on Medical Physics and Biomedical Engineering 2000 (available at http://dmnu-pet5.hcuge.ch).
23. Zaidi H. Relevance of accurate Monte Carlo modeling in nuclear medical imaging. Med Phys 1999;26:574-608.

24. Zaidi H, Scheurer AH, Morel C. An object-oriented Monte Carlo simulator for 3D cylindrical positron tomographs. Comput Methods Programs Biomed 1999;58:133-145.
25. Hudson HM, Larkin RS. Accelerated image reconstruction using ordered subsets of projection data. IEEE Trans Med Imag 1994;13:601-609.
26. Jacobson M, Levkovitz R, Ben-Tal A, et al. Enhanced 3D PET OSEM reconstruction using inter-update Metz filtering. Phys Med Biol 2000;45:2417-2439.
27. Labbe C, Thielemans K, Zaidi H, Morel C. An object-oriented library incorporating efficient projector/back-projector operators for 3D PET reconstruction. Proceedings of the International Meeting on Fully Three-dimensional Image Reconstruction in Radiology and Nuclear Medicine (3D'99), Egmond aan Zee, Netherlands 23-26 June 1999, pp 137-140.
28. Hoffman EJ, Cutler PD, Digby WM, Mazziotta JC. 3-D phantom to simulate cerebral blood flow and metabolic images for PET. IEEE Trans Nucl Sci 1990;37:616-620.
29. Townsend DW, Choi Y, Sashin D, Mintun MA. An investigation of practical scatter correction techniques for 3D PET. J Nucl Med 1994;35:50P.
30. Kinahan PE, Rogers JG. Analytic 3D image reconstruction using all detected events. IEEE Trans Nucl Sci 1989;36:964-968.
31. Townsend DW, Wensveen M, Byars LG, et al. A rotating PET scanner using BGO block detectors: design, performance and applications. J Nucl Med 1993;34:1367-1376.
32. Levin CS, Dahlbom M, Hoffman EJ. A Monte Carlo correction for the effect of Compton scattering in 3-D PET brain imaging. IEEE Trans Nucl Sci 1995;42:1181-1188.
33. Hutton BF, Baccarne V. Efficient scatter modelling for incorporation in maximum likelihood reconstruction. Eur J Nucl Med 1998;25:1658-1665.